DOI: 10.61782/fa.2023.0107

forum acusticum 2023

FREE-FIELD SOUND RADIATION MEASUREMENT WITH PHOTOGRAMMETRY

Paolo Gardonio[1*] **Gianluca Guernieri**[1] **Emanuele Turco**[1] **Dal Bo Loris**[1]
Roberto Rinaldo[1] **Andrea Fusiello**[1]
[1] DPIA, Università degli Studi di Udine, Via delle Scienze 206 – 33100, Udine, Italy
[*] paolo.gardonio@uniud.it

ABSTRACT

This paper presents a new methodology for the measurement of the free-field sound radiation produced by the vibrations of machines and structures. The idea is to reconstruct the vibration field of the machine/structure from triangulation of video acquisitions. The free-field sound radiation is then derived from the classical boundary integral formulation. The proposed measurement approach is described for the sound radiation generated by the flexural vibrations of a baffled panel. The panel is divided into a grid of radiating elements whose centres are denoted by small dots bonded on the panel. The transverse vibrations of the panel at the centres of the dots are estimated via triangulation from the video acquisitions of six cameras. Finally, the free-field sound radiation is reconstructed from the Rayleigh integral, which is approximated into a finite sum over the grid of elements. The study has considered the sound radiation produced by the flexural deflection shapes generated by a tonal force excitation at the first five resonance frequencies of the plate.

Keywords: *sound radiation measurement, vibration measurement, photogrammetry, multi-camera, multi-view.*

1. INTRODUCTION

In practice, the measurement of sound radiation from machinery and sound transmission through partitions involves advanced measurement setups encompassing calibrated sensors, multi-channel acquisition/signal-conditioning systems and multi-channel spectral analysers. Moreover, it may require expensive facilities (e.g. reverberant rooms and/or anechoic chambers). In fact, two measurement methodologies are normally employed to generate accurate measurements [1-6]. The first relies on the so-called in-situ measurements such that the sound radiation/transmission is measured on the site where the device/partition is installed using phonometers, acoustic cameras, sound intensity probes, etc. Instead, the second expects the machinery or partitions are installed in specific sound-radiation/sound-transmission suites, such that the sound radiation/transmission is measured in a controlled environment, normally with arrays of microphones or a single rotating boom microphone. The in-situ measurements are rather delicate to perform since they are normally affected by flanking noise sources, uncontrolled sound reflection effects, uncertainty of the machinery / wall operation conditions and low repeatability of the measurement arrangement. The measurements in specially dedicated sound radiation / transmission suites are not affected by such issues; however, they require quite a lot of efforts, too, since the machinery or wall partition should be moved and carefully installed in the reverberant / anechoic room or reverberant-reverberant / reverberant-anechoic sound transmission facility.

This paper presents a short overview of a new sound radiation / transmission measurement approach based on video camera acquisitions, which has been presented in [7,8] and therein references. The methodology is based on multiple-cameras video acquisitions. The full-field flexural vibration of the tested machinery / wall is then reconstructed through three-dimensional point tracking and triangulation [9-12]. The sound radiation is finally derived with the Kirchhoff-Helmholtz integral formulation [13]. In this paper, a simple case-study is considered, which encompasses a thin rectangular plate clamped on a rigid

[*] ***Corresponding author***: paolo.gardonio@uniud.it.

frame. The flexural vibration and sound radiation fields are derived with the proposed camera-based methodology for time-harmonic vibrations generated by a tonal force exerted on the plate by a shaker.

2. EXPERIMENTAL SETUP

Figs. 1a,b show the steel thin rectangular plate model-structure, which is clamped on a rigid frame that works as a small baffle. The plate is excited by a point force exerted by a shaker, which has been connected to the plate via a stinger equipped with a force cell. As highlighted in Fig. 1b, the plate has been divided into a mesh of $N_w = 11 \times 7 = 77$ quadrilateral elements whose centres have been highlighted with yellow dots (markers) bonded directly on the plate.
As can be noticed in Fig. 1a, a truss structure has been placed in front of the plate, which has been used to hold the six cameras with the optical axis pointing to the centre of the plate. Table 1 reports the principal parameters of the plate and cameras experimental setup.

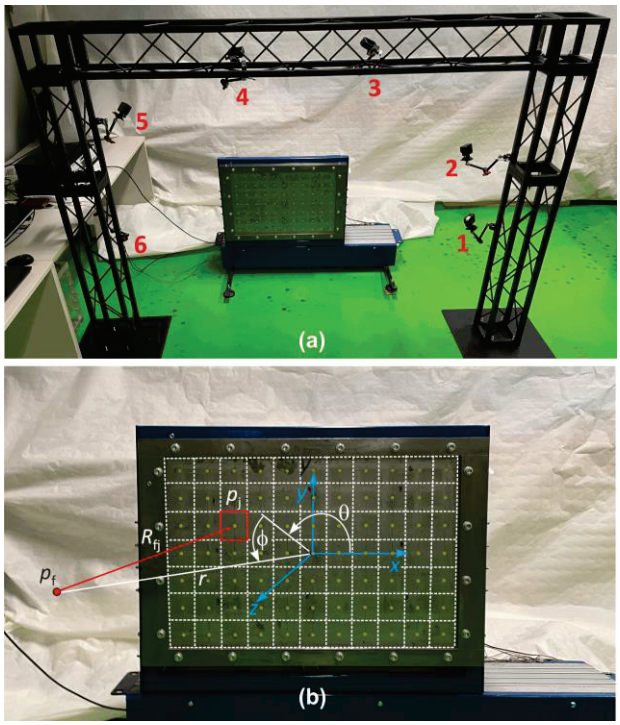

Figure 1. (a) Plate and truss structure with the 6 cameras setup. (b) Mesh of radiating pistons with the yellow circular markers at their centres.

Table 1. Experimental setup.

Parameter	Value
Plate dimension	$l_{xp} \times l_{xp} = 668 \times 443$ mm
Plate thickness	$h_p = 1.8$ mm
Plate material	steel
Position shaker	$x_p, y_p = -86, -111$ mm
First 5 res. Freq.	33, 51, 86.5, 91, 111.8 Hz
Camera model	Gopro Hero 10
Camera CCD sensor	1/2.3" (6.17 × 4.55 mm)
Camera spatial res.	2704 × 1520 fps
Camera temporal res.	240 fps
Positions of cameras	$r_1 = 1.25$ m, $\theta_1 = 25^o$, $\phi_1 = 10^o$
	$r_2 = 1.33$ m, $\theta_2 = 27^o$, $\phi_2 = 30^o$
	$r_3 = 1.28$ m, $\theta_3 = 50^o$, $\phi_3 = 57^o$
	$r_4 = 1.20$ m, $\theta_4 = 116^o$, $\phi_4 = 60^o$
	$r_5 = 1.30$ m, $\theta_5 = 151^o$, $\phi_5 = 40^o$
	$r_6 = 1.30$ m, $\theta_6 = 160^o$, $\phi_6 = 20^o$

3. CAMERA MEASUREMENTS AND IMAGE PROCESSING

The measurement campaign with the six cameras was implemented in three principal phases: initially, the cameras were calibrated, then the videos were acquired with the six cameras suitably synchronised and, finally, the recordings were post-processed to find the markers positions in each image. Overall, as detailed in [7,8], the following sequence of steps were implemented.

- **Cameras calibration** – To start with, each camera was calibrated according to the Sturm-Maybank-Zhang method [14,15] and ensuring compensation of the radial distortion generated by the optics of the cameras.
- **Video acquisitions** – Synchronized videos were then acquired with the plate excited by a tonal force at the 5 resonance frequencies of the plate flexural vibration.
- **Frames extraction** – Hence, 6 coherent sequences of frames were extracted from the videos of the 6 cameras.
- **Perspective rectification** – Then, a 2D transformation H_i, named homography, was applied to each image of the recordings to remove perspective effects.
- **Tentative markers detection** – At this point, a coarse identification of the markers centre coordinates was carried out on the rectified frames with a classical template matching technique, which is also known as the cross-correlation technique.
- **Markers validation** – To avoid errors arising from false marker-like spots in the images, the Hungarian method [16] was then applied to ensure the markers tentative coordinates were in the vicinity of their rest coordinates.

- **Triangulation** – Once the image plane centre coordinates of the markers had been identified for each frame of the 6 recordings, the 3D positions of the markers were reconstructed from triangulation as detailed below.

In general, for a given frame instant t_k, a given camera *i* and a given marker *j*, the physical 3D mm-coordinates of the marker $\mathbf{M}_j(t_k) = [X_j(t_k) \quad Y_j(t_k) \quad Z_j(t_k)]^T$ are linked to its image 2D pixel-coordinates on the *i*-th camera $\mathbf{m}_j^i(t_k) = [u_j(t_k) \quad v_j(t_k)]^T$ by the perspective projection equation [9]:

$$\mathbf{m}_j^i(t_k) = f\left(\mathbf{M}_j(t_k), \mathbf{g}_j\right), \tag{1}$$

where the vector $\mathbf{g}_j$ contains the extrinsic parameters of the *i*-th camera. A technique called Bundle Adjustment (BA) [17], simultaneously recovers the exterior orientation of the two cameras and the markers centre coordinates by solving a non-linear least squares problem, which turns into minimising the cost function

$$\sum_{i,j} \left\| \mathbf{m}_j^i(t_k) - f\left(\mathbf{M}_j(t_k), \mathbf{g}_j\right) \right\|_2^2, \tag{2}$$

with reference to both $\mathbf{M}_j(t_k)$ and $\mathbf{g}_j$. The BA computes only one set of unknowns when the other is given, and thus it will be referred as a partial BA. The minimisation of this cost function is carried out iteratively with the Levenberg–Marquardt algorithm. To initialise the exterior orientation of the cameras, six separate resections were implemented with the Direct Linear Transform algorithm (DLT) [17,18] using both the image coordinates of the markers detected in a rest frame $\mathbf{m}_j^i(t_0)$ acquired with no vibrations of the plate and the nominal rest coordinates of the markers $\mathbf{M}_j(t_k)$. The actual computation of the markers 3D centre coordinates $\mathbf{M}_j(t_k)$ at each instant t_k was implemented in the final BA, which comprises all the frames of all the cameras, with the exterior orientation of the cameras, too, considered among the unknowns. The initialisation exploited the nominal rest coordinates of the centres of the markers and the exterior orientation derived in the previous step. It should be highlighted here that, in principle, two cameras only are required to perform triangulation. Nevertheless, as discussed in Ref. [19], a greater number of camera measurements leads to more accurate results. The camera calibration, image processing and triangulation post-processing tasks described above were all implemented in MatLab using routines from Ref. [20].

4. RECONSTRUCTION OF VIBRATION FIELD FROM CAMERA MEASUREMENTS

For the thin flat plate at hand, the small-amplitude flexural (transverse) displacements at the centre of the j-th marker can be suitably derived its $Z_j(t_k)$ coordinate obtained from the BA described above. Indeed, assuming time-harmonic vibrations with circular frequency ω, the transverse displacement at the centre of the *j*-th marker was taken equal to [7,8]

$$w(x_j, y_j, t_k) \cong \mathrm{Re}\left\{w_0(x_j, y_j, \omega) e^{j(\omega t_k + \varphi_0(x_j, y_j, \omega))}\right\}, \tag{3}$$

where $w_0(x_j, y_j, \omega)$ and $\varphi_0(x_j, y_j, \omega)$ are the amplitude and phase of the displacement at each marker point. Since the cameras are operated at a frame rate $1/T$, the amplitude and phase terms, $w_0(x_j, y_j, \omega)$ and $\varphi_0(x_j, y_j, \omega)$, were derived from the sequence of *z*-coordinates $Z_j(t_k)$ of the *j*-th marker centre position assuming $k = 0, \cdots, N-1$. For instance, the data length N was selected in such a way as the sequence contains an integral number of periods of the sinusoid. In this case, the coefficients of the Discrete Fourier Transform (DFT) of the $Z_j(t_0), Z_j(t_1), \cdots, Z_j(t_{N-1})$ time-history, processed for example with a Fast Fourier Transform (FFT) algorithm, gave exactly the required modulus and phase values [21].

At this point, having the plate vibration field, the sound radiation was derived straightforwardly with the Kirchhoff-Helmholtz integral formulation [13]. For the baffled plate at hand, this integral equation specialises into the so-called Rayleigh integral [13] such that, as shown in Refs. [7,8], the sound pressure at a given position (x_f, y_f, z_f) was approximated in terms of the following Riemann sum:

$$p(x_f, y_f, z_f, t_k) \cong \mathrm{Re}\left\{\frac{-\omega^2 \rho S_0}{2\pi} \sum_{j=1}^{N_w} \frac{w_0(x_j, y_j, \omega) e^{jkR_{fj}}}{R_{fj}} e^{j(\omega t_k + \varphi_0(x_j, y_j, \omega))}\right\} \tag{4}$$

Here S_0 is the area of the radiating elements, $N_w = 11 \times 7 = 77$ is the number of markers depicted on the plate, $w_0(x_j, y_j, \omega)$ and, as highlighted in Fig. 1b,

$$R_{fj} = \sqrt{(x_f - x_j)^2 + (y_f - y)^2 + z_f^2} \tag{5}$$

is the distance between the free-field point (x_f, y_f, z_f) and the centre of the *j*-th marker (x_j, y_j).

5. EXPERIMENTAL RESULTS

Figs. 2 and 3 show the flexural vibration and sound radiation fields reconstructed from the cameras video acquisitions when the plate is excited harmonically at the first five resonance frequencies. The flexural vibration fields at the first, second and fifth resonance frequencies are controlled by the (1,1), (2,1) and (2,2) flexural natural mode shapes respectively. Also, when the plate is excited harmonically at the third and fourth resonance frequencies, the flexural vibration fields are characterised respectively by the mode shape (1,2) mixed with the (3,1) mode shape and by the mode shape (3,1) mixed with the (1,2) shape. This is because, the third and fourth resonance frequencies

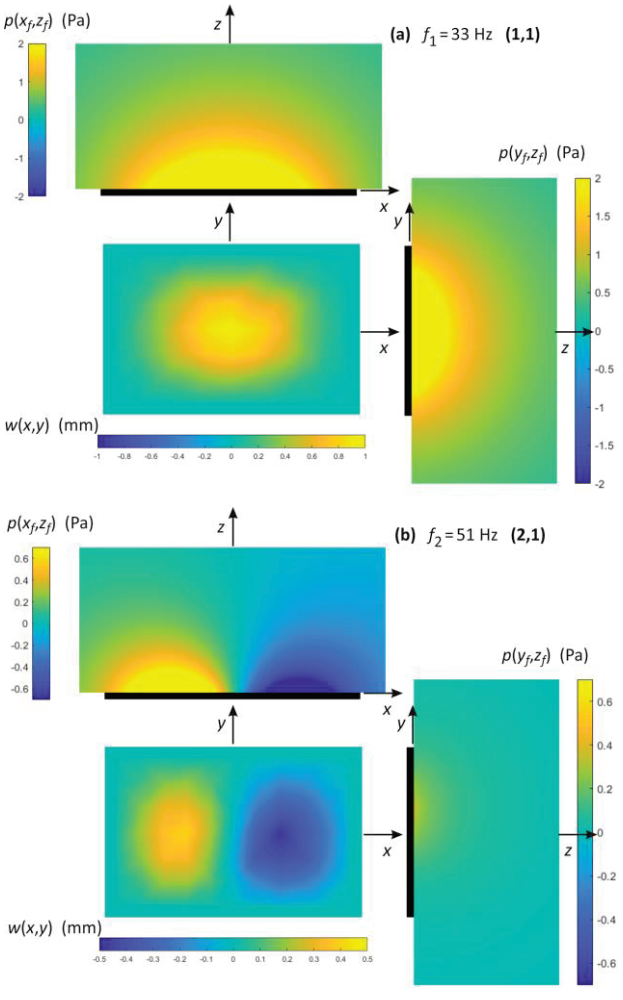

Figure 2. Vibration and acoustic fields reconstructed from the camera measurements at f_1, f_2.

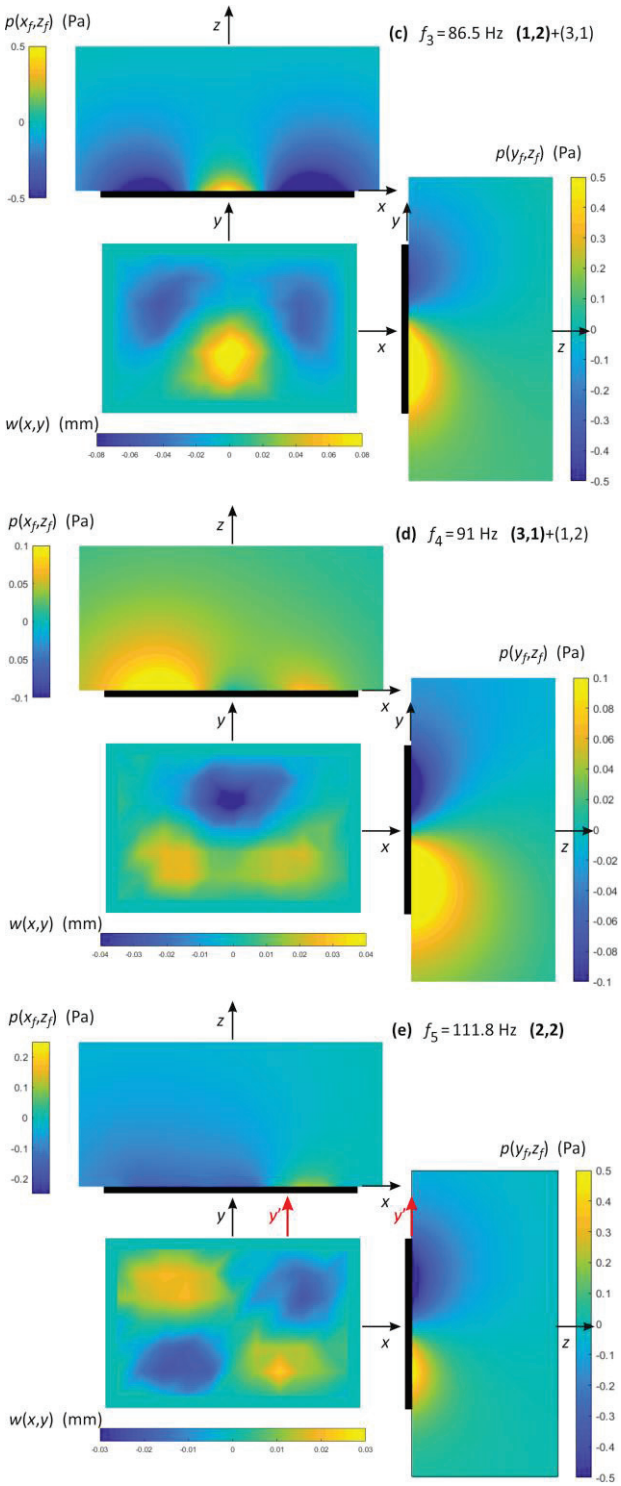

Figure 3. Vibration and acoustic fields reconstructed from the camera measurements at f_3, f_4, f_5.

are quite close to each other and thus the two resonant responses are characterised by the superposition of a "principal" resonant mode and a "neighbour" off-resonant mode. In general, the flexural vibration fields are slightly distorted by the nearfield vibration effect generated by the point force excitation [22].

Moving to the sound radiation, Figs. 2 and 3 show that the estimated acoustic fields replicate quite closely the near-fields that would be generated by the time-harmonic flexural vibrations of the plate at the first five resonance frequencies. For example, when the plate vibrates at $f_1 = 33$ Hz, such that the flexural response is controlled by the shape of the (1,1) mode, as one would expect, the sound radiation is characterised by a monopole-like acoustic field. Likewise, when the plate vibrates at $f_2 = 51$ Hz, such that the flexural response is controlled by the shape of the (2,1) mode, the sound radiation shows the typical dipole-like acoustic field, which is characterised by two-lobes on the *xz* plane and, due to acoustic destructive interference, by negligible acoustic pressures on the *yz* plane. A similar acoustic field is found when the plate vibrates at $f_5 = 111.8$ Hz. Here the flexural response is controlled by the (2,2) mode. Thus, the sound radiation is characterised by a quadrupole-like field, which, due to destructive interference, results into negligible acoustic pressures on both the *xz* and *yz* planes. However, considering the quarter span *y'z* plane shown in Figure 3c, the sound field is characterised by the expected two-lobes structure. Finally, when the plate vibrates at $f_3 = 86.5$ Hz and $f_4 = 91$ Hz such that the flexural response is characterised by combinations of the the (1,2) and (3,1) modes, the sound radiation on the *xz* and *yz* planes show respectively two and three lobes.

To conclude, it should be highlighted here that the results presented in this paper were compared in Ref. [8] with flexural vibration measurements taken with a laser vibrometer and with sound radiation measurements taken with an array of microphones. It was found that the vibration and acoustic fields reconstructed from the camera measurements satisfactorily replicate those measured with the laser vibrometer and microphone array. Overall, the cameras-reconstructed flexural vibration fields and sound radiation fields at the first five resonance frequencies are characterised by 7.6 – 25.4% and 2.8 – 25.5% mean errors with respect to the fields measured with the laser vibrometer and microphone arrays respectively. These values should be handled with care, since part of the errors may be ascribed to the vibro-acoustic measurements themselves. In particular, the sound radiation was measured on a laboratory room rather than in a anechoic room. Moreover, the back radiation from the plate was not properly shielded. Nevertheless, qualitatively, the vibration and sound radiation fields reconstructed from the camera measurements closely replicated the fields measured with the laser vibrometer and array of microphones.

6. CONCLUSIONS

This paper has presented a new methodology for the derivation of the flexural vibration field and the sound radiation field of a structure from camera measurements. Initial tests taken with six cameras on a thin plate model structure excited in bending by a tonal force at the first five resonance frequencies, have shown that the proposed approach generates accurate estimates of both the vibration and sound radiation fields.

The results presented in this paper have been generated using off the shelf cameras, with limited spatial and time resolutions for vibro-acoustic measurements. Indeed, it should be emphasised that to cover the typical frequency ranges of acoustic measurements in air (i.e. several kHz), and to properly reconstruct the vibration and sound radiation fields both at resonance and off-resonance frequencies (which may differ by 20 to 40 dB, that is 1 or 2 order of magnitude), the camera should exhibit both high frame-rate and high spatial-resolution characteristics. In this respect, new image acquisition technologies have been recently commercialised, which should guarantee the time and spatial resolutions necessary to implement the vibro-acoustic measurement approach proposed in this paper.

It is therefore expected the proposed methodology can be suitably adapted to reproduce typical measurements of sound radiation from machines and the measurements of sound transmission through partitions respectively in terms of radiation Sound Power Level (SPL) and Transmission Loss factor (TL) narrow-band and third-octave-band spectra as outlined by the appropriate ISO guidelines (e.g. Refs. [4,6]).

7. REFERENCES

[1] R. F. Barron: *Industrial Noise Control and Acoustics*. New York: Marcel Dekker Inc., 2003.

[2] D. A. Bies, C. H. Hansen: *Engineering Noise Control Theory and Practice*. London: Spon Press, 2009.

[3] F. Fahy, *Measurement of audio-frequency sound in air*, in: *Fundamentals of Sound and Vibration*. London: CRC Press, 2015.

[4] Acoustics: *Determination of sound power levels of noise sources – Guidelines for the use of basic standards*, ISO 3740:2019, 2019.

[5] E. Petersen: *An Overview of Standards for Sound Power Determination, Application Note*. Bruel & Kjear Instruments, BO 0416 - 12, 1995.

[6] Acoustics: *Measurement of sound insulation in buildings and of building elements using sound intensity - Part 1: Laboratory measurements; -Part 2: Field measurements; Part 3: Laboratory measurements at low frequencies*, ISO 15186-1:2000, 2000.

[7] P. Gardonio, R. Rinaldo, L. Dal Bo, R. Del Sal, E. Turco, A. Fusiello: "Freefield sound radiation measurement with multiple synchronous cameras," *Measurement*, Vol. 188, 2022.

[8] P. Gardonio, G. Guernieri, E. Turco, L. Dal Bo, R. Rinaldo, A. Fusiello: "Reconstruction of the sound radiation field from flexural vibrations measurements with multiple cameras," *Mechanical Systems and Signal Processing*, Vol. 195, 2023.

[9] A. Gruen: "Fundamentals of videogrammetry - a review," Hum. Mov. Sci. 16, pp. 155–187, 1997.

[10] J. Baqersad, P. Poozesh, C. Niezrecki, P. Avitabile: "Photogrammetry and optical methods in structural dynamics – a review," *Mech. Syst. Signal Pr.* Vol. 86, pp 17–34, 2017.

[11] S. Park, H. Park, J. Kim, H. Adeli: "3d displacement measurement model for health monitoring of structures using a motion capture system," *Measurement*. Vol. 59, pp 352–362, 2015.

[12] D. Gorjup, J. Slavic, M. Boltezar: "Frequency domain triangulation for full-field 3D operating-deflection-shape identification," *Mech. Syst. Signal Pr.* Vol. 133, pp 143–152, 2019.

[13] F. Fahy, P. Gardonio: *Sound and Structural Vibration. Radiation, Transmission and Response*, 2nd Ed., London: Academic Press, 2007.

[14] P. F. Sturm and S. J. Maybank: "On plane-based camera calibration: A general algorithm, singularities, applications," in *Proceedings. IEEE Computer Society Conference on Computer Vision and Pattern Recognition (Cat. No PR00149)*, 1999, Vol. 1, pp. 432-437, 1999.

[15] Z. Zhang: "A flexible new technique for camera calibration," *IEEE Trans Pattern Anal Mach Intell*, Vol. 22, No. 11, pp. 1330–1334, 2000.

[16] H. W. Kuhn: "The Hungarian method for the assignment problem," *Naval Research Logistics Quarterly*, vol. 2, No. 1–2, pp. 83–97, 1955.

[17] R. Hartley, A. Zisserman: *Multiple View Geometry in Computer Vision*, Cambridge: Cambridge University Press, 2004.

[18] I. Sutherland: "Three-dimensional data input by tablet," *Proc. IEEE* Vol. 62, No. 4, pp 453–461, 1974.

[19] R. Del Sal, L. Dal Bo, E. Turco, A. Fusiello, A. Zanarini, R. Rinaldo, P. Gardonio: "Structural vibration measurement with multiple synchronous cameras," *Mechanical Systems and Signal Processing*, Vol. 157, 2021

[20] A. Fusiello: "Computer Vision Toolbox for Matlab" *https://github.com/fusiello/Computer_Vision_Toolkit*, 2022.

[21] A. V. Oppenheim, R. W. Schafer: *Discrete-Time Signal Processing*, 3rd Edition, Prentice Hall Press, 2009.

[22] L. Cremer, M. Heckl: *Structural Vibrations and Sound Radiation at Audio Frequencies*. Berlin, Springer-Verlag, 1988.